We are IntechOpen, the world's leading publisher of Open Access books
Built by scientists, for scientists

6,900
Open access books available

186,000
International authors and editors

200M
Downloads

Our authors are among the

154
Countries delivered to

TOP 1%
most cited scientists

12.2%
Contributors from top 500 universities

CLARIVATE ANALYTICS
BOOK CITATION INDEX
INDEXED

WEB OF SCIENCE™

Selection of our books indexed in the Book Citation Index
in Web of Science™ Core Collection (BKCI)

Interested in publishing with us?
Contact book.department@intechopen.com

Numbers displayed above are based on latest data collected.
For more information visit www.intechopen.com

Structural Engineering on Pt-Free Electrocatalysts for Dye-Sensitized Solar Cells

Yi-June Huang, Han-Ting Chen, Shiuan-Bai Ann, Chun-Ting Li and Chuan-Pei Lee

Abstract

In recent decades, plenty of nanomaterials have been investigated as electrocatalysts for the replacement of the expensive platinum (Pt) counter electrode in dye-sensitized solar cells (DSSCs). The key function of the electrocatalyst is to reduce tri-iodide ions to iodide ions at the electrolyte/counter electrode interface. The performance of the electrocatalyst is usually determined by two key factors, i.e., the intrinsic heterogeneous rate constant and the effective electrocatalytic surface area of the electrocatalyst. The intrinsic heterogeneous rate constant of the electrocatalyst varies by different types of materials, which can be roughly divided into five groups: non-Pt metals, carbons, conducting polymers, transition metal compounds, and their composites. The effective electrocatalytic surface area is determined by the nanostructure of the electrocatalyst. In this chapter, the nanostructural design and engineering on different types of Pt-free electrocatalysts will be systematically introduced. Also, the relationship between various nanostructures of electrocatalysts and the pertinent physical/electrochemical properties will be discussed.

Keywords: counter electrode, dye-sensitized solar cells, electrocatalyst, nanostructure
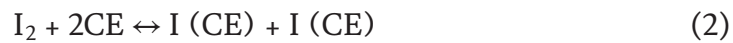
1. Introduction

### 1.1 Dye-sensitized solar cells (DSSCs)

Fossil fuel, as a limiting energy source, may be run out in the upcoming centuries. However, the consumption of energy increases every year [1, 2]. As a result, finding and developing renewable energy sources is an urgent problem. Due to the unlimitedness of renewable energy resources, they are candidates to be reliable replacement for sustainable usage in the future. Among them, the Sun has been considered as one of the most promising renewable energy sources. It provides about 120,000 terawatts to the earth, which equals thousand times of the current energy consumption rate. The solar cells can utilize the sunshine and transform to electricity [3–5]. Generally, solar cells can be classified to four generations: the first generation is silicon-based solar cells; the second generation is CIGS (CuInGaSe), CZTS (CuZnTiSe), and CdTe solar cells; the third generation is organic photovoltaics (OPVs) and dye-sensitized solar cells (DSSCs); and the fourth generation is

perovskite solar cells (PSCs). The first and second generations have been widely explored for decades, and they are the most common solar cells at present. However, they are fabricated through expensive, toxic, energy-intensive, high-temperature, and high-vacuum processes. Therefore, DSSCs are very competitive to the first and second generations of solar cells due to numerous advantages including easy fabrication, low cost (**Figure 1**) [3], and high performance at dim-light condition. Moreover, DSSCs can be used in indoor ambient applications [5–9].

A DSSC is composed of a photoanode, electrolyte, and counter electrode (CE), as shown in **Figure 2**. When a photoanode is excited by the sun or photon, it will release the electron to the external circuit. At the same time, the iodide/triiodide (I^-/I_3^-) redox couple will relax the photoanode to its ground state. Then the CE will reduce the redox couple to regenerate the DSSC. Among them, the CE plays an important role to determine the DSSC performance [10]. At the CE/electrolyte interface, the electrochemical mechanism goes through I_3^- decomposition (Eq. (1)) → adsorption (Eq. (2)) → catalytic reduction reaction (Eq. (3)) → desorption (Eq. (4)), and the overall reaction shows as Eq. (5) [11]. Among these reaction steps, Eq. (3) is found to be the slowest step, which means the rate-determining step to decide the DSSC performance.

$$I_3^- \leftrightarrow I_2 + I^- \tag{1}$$

$$I_2 + 2CE \leftrightarrow I\,(CE) + I\,(CE) \tag{2}$$

$$I\,(CE) + e^- \leftrightarrow I^-\,(CE) \tag{3}$$

$$I^-\,(CE) \leftrightarrow I^- + CE \tag{4}$$

$$I_3^- + 2e^- \leftrightarrow 3I^- \tag{5}$$

There are two ways to enhance the electrocatalytic reduction reaction. One is to increase the heterogeneous rate constant, relating to the intrinsic electrocatalytic ability of the electrocatalyst. The other is to engineer the structure of the electrocatalyst for I_3^- reduction with regard to the charge transfer route and the surface area. To replace a traditional platinum (Pt) electrocatalyst, where Pt is a rare and expensive
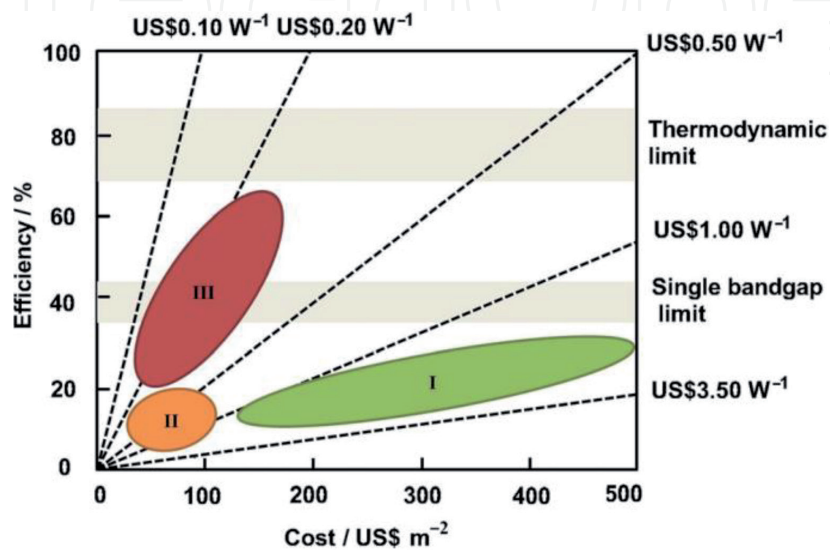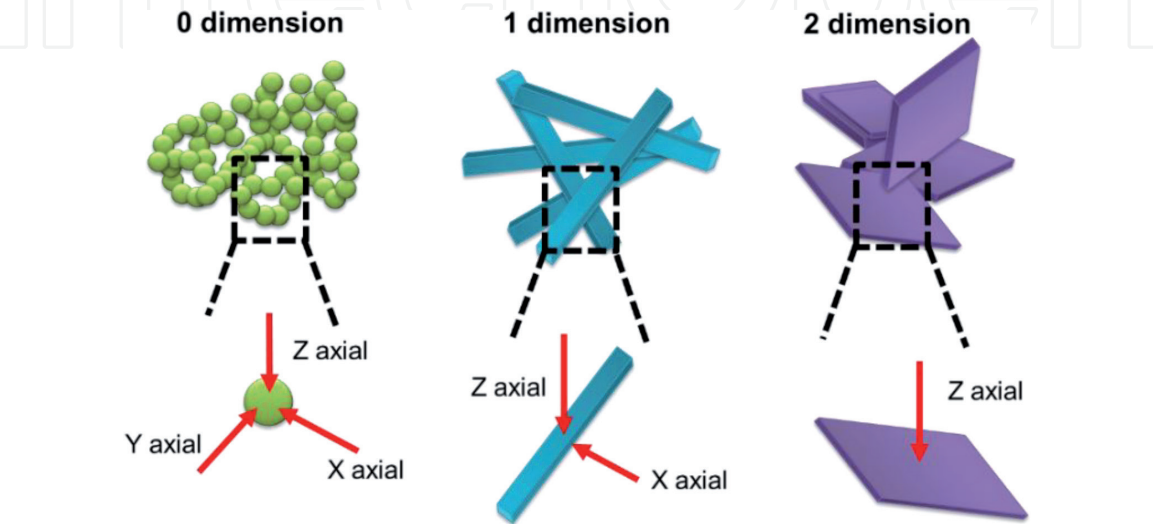

Figure 1.
Efficiency and cost projection for first- (I), second- (II), and third-generation (III) photovoltaic technology [3].
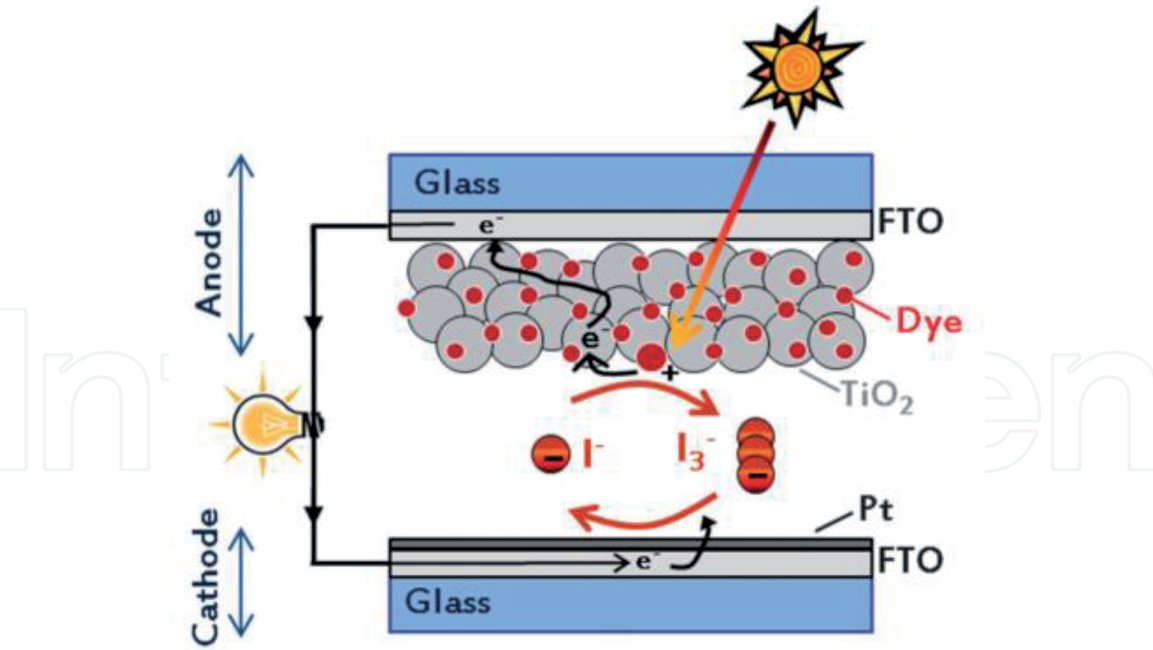
Figure 2.
The structure and mechanism of DSSCs [2].

element, several types of materials, such as carbon materials [5, 12–28], conductive polymers [29–48], and transition metal compounds [37, 45, 49–79] have been extensively explored to elevate the cell efficiency (η) and decrease the cost of the CEs.

To date, there have been a very limited number of non-Pt nanomaterials that could have a comparable intrinsic heterogeneous rate constant to that of Pt. However, the specific structural designs of nanomaterials would largely increase the effective electrocatalytic surface area so as to provide better overall electrocatalytic ability than Pt. Moreover, the nanostructured electrocatalysts could have appropriate interfacial affinity, good electrochemical stability, or specific self-assembly natures; these properties may influence the DSSC performance as well. A typical nanostructured material can be defined if any dimension of the material is lower than 100 nm. The nanostructured material can be classified into three groups: zero-dimensional (0D, e.g., nanoparticle, nanocube, etc.), one-dimensional (1D, e.g., nanorod, nanotube, nanoneedle, etc.), and two-dimensional (2D, e.g., nanosheet, nanopental, etc.) structures, as shown in **Figure 3**. Generally, 0D structure is

Figure 3.
The scheme of zero-dimensional (0D), one-dimensional (1D), and two-dimensional (2D) structure.

expected to supply the high electrochemical surface area, and 1D/2D structures are claimed to have directional electron transfer pathways. In this chapter, different strategies of designing nanostructured carbon materials, conductive polymers, and transition metal compounds to increase their active surface area/charge transfer route will be systematically discussed. The corresponding DSSC performance is also included.

2. Nanostructure materials of counter electrode

2.1 Carbon materials

Carbon materials, composed of carbon atoms having sp^2-hybridization (e.g., graphite, graphene, graphene oxide, and carbon nanotube) or sp^3-hybridization (e.g., carbon black and activated carbon), have been widely investigated as the CEs due to their material specialties such as low cost, high electrical conductivity, high thermal stability, and good corrosion resistance [3, 4, 80–84]. The carbon materials with sp^2-hybridization normally exhibit a 1D or 2D structure, and those with sp^3-hybridization have a 0D structure. However, carbon materials often exhibit serious aggregation that reduces the material conductivity and limits the electrochemical surface area. Here we include several studies which provided practical strategies to overcome this problem and reach comparable/better cell efficiencies than the Pt-incorporated DSSCs, as listed in **Table 1**.

For example, Fan et al. used a small 0D porous carbon nanoball (diameter = 20 ± 3 nm) to assemble a large 0D hollow nanoball (diameter = 100 ± 10 nm), as shown in **Figure 4(a)** [12]. Tseng et al. introduced a one-step synthetic method to make tens of 2D nitrogen-doped graphene with a thickness of ~3.5 nm stacking together to form a building block as a 0D hollow nanoball, as shown in **Figure 4(b)** [22]. Fan et al. used a small 0D porous carbon nanoball (diameter = 20 ± 3 nm) to assemble a large 0D hollow nanoball (diameter = 100 ± 10 nm), as shown in **Figure 4(b)** [12]. The hollow nanoballs consisting of nitrogen-doped graphene and porous carbon gave their DSSCs ηs of 7.53 and 8.67%, respectively, which were comparable to the Pt-based cells. Besides, nitrogen-doped graphene (**Figure 4(c)**, 7.07%) [13] and the wrinkled 2D graphene (**Figure 4(d)**, 7.80%) [14] nanosheets were used to form a honeycomb-like structure having extra surface area and vertically aligned sub-nanosheets as the additional electron transfer routes.

| Materials	η (%)	η of Pt (%)	Structure	Ref
Porous carbon	8.67	9.34	Hollow nanoball	[12]
Nitrogen-doped graphene	7.53	7.70	Hollow nanoball	[22]
Nitrogen-doped graphene	7.07	7.44	Honeycomb	[13]
Graphene	7.80	8.00	Honeycomb	[14]
Carbon nanotubes and graphene	8.2	6.4	Nanotube vertically fused onto the nanosheet	[15]
Carbon nanotube and N-doped graphene	8.31	7.56	Nanotube intertwined with nanosheet	[16]
Carbon nanotube and graphene oxide	6.91	7.26	Nanotube embedded in nanosheet	[27]

Table 1.
A partial list of literature on the DSSCs with carbon material-based CEs.
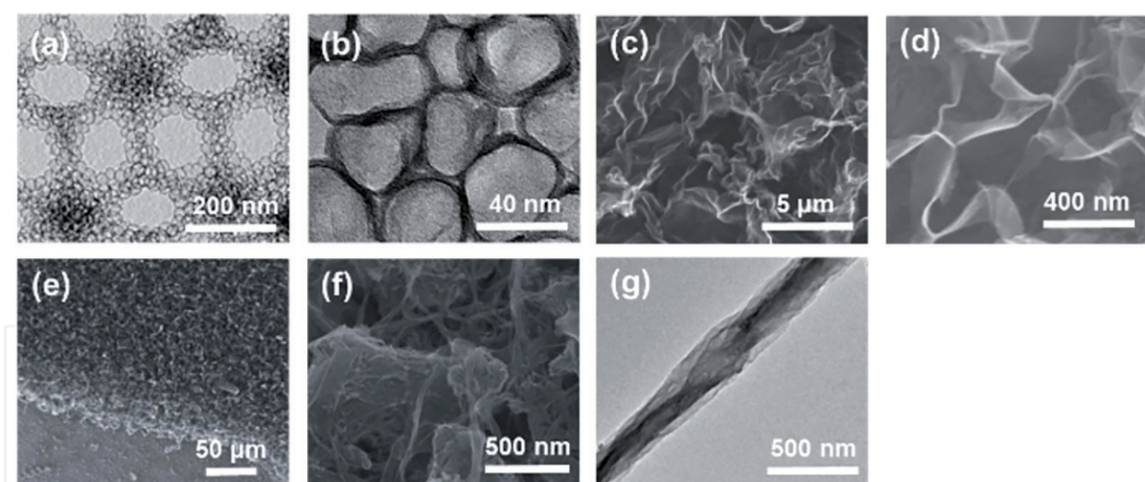
Figure 4.
The structures of carbon materials including (a and b) hollow nanoball [12, 22], (c) nanosheet [13],
(d) honeycomb [14], and (e–g) nanotube with nanosheet [15, 16, 27].

The combination of few kinds of carbon materials was reported to form a hierarchical structure, which could not only create a high surface area but also a directional electron transfer pathway. Dong et al. made 1D few-walled carbon nanotubes (CNTs, tens of microns long) vertically fuse onto the 2D graphene nanosheet (<1 nm thick), as shown in **Figure 4(e)** [15]. The red seven-membered rings at the neck seamlessly fuse the tubular CNTs to the planar graphene without obvious CNT aggregation (**Figure 5(a)**). Even though the CNTs only covered few parts of the electrode surface, they still benefited the electrolyte wetting and electron transfer rate within the counter electrode, leading to a better η (8.2%) than the Pt-based cell (6.4%). Ma et al. reported a similar hierarchical structure, where the single-walled carbon nanotube (SWCNT) was located on a flat N-doped graphene (N-doped GN) nanosheet by the z-axis direction (**Figure 4(f)**) [16]. As a result, composite SWCNT@N-doped GN reached higher η (8.31%) than Pt (7.56%). Yeh et al. prepared a hybrid heterostructure of multiwalled carbon nanotube (MWCNT, diameter = 15 nm) and reduced graphene oxide (rGO, thickness = 25 nm) nanosheet, where the 2D rGO nanosheet-like shell was wrapped around the 1D CNT core (**Figure 4(g)**) [27]. In the MWCNT@rGO composite material, the tubular MWCNTs functioned as the 1D heterogeneous electron transfer pathways, which provided sufficient electrons to the electrochemical reaction; at the same time, the 2D rGO nanosheet supplied multiple edges as the active sites to reduce I_3^- to I^- (**Figure 5(b)**). The hybrid heterostructure of MWCNT@rGO was found to avoid
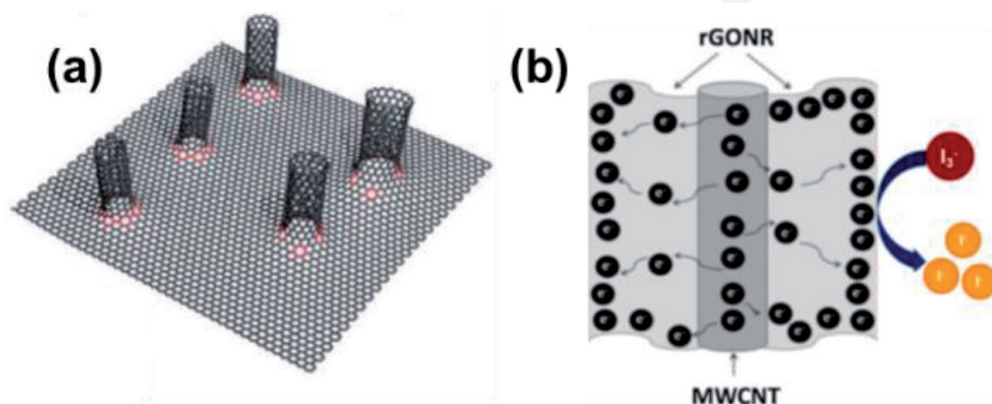
Figure 5.
The scheme of hierarchical structures of (a and b) nanotube with nanosheet [15, 27].

the aggregations among the MWCNTs or among the rGOs. Thus, the MWCNT@ rGO rendered its DSSC an η of 6.91%, which is close to the Pt-based cell (7.26%).

2.2 Conductive polymer materials

Since 2000, the conductive polymer material has been discovered by Shirakawa, MacDiarmid, and Heeger [29]. Conductive polymers have attracted much attention as DSSC CEs owing to their excellent conductivity, good adhesion to the substrate, easy fabrication, light-weight, and good accessibility in terms of roll-to-roll processing. Common conductive polymers include poly(3,4-ethylenedioxythiophene) (PEDOT) [30, 35, 36, 40–43], poly(3,4-ethylenedioxythiophene)-poly(styrene sulfonate) (PEDOT:PSS) [30, 43, 48], poly(hydroxymethyl 3,4-ethylene-dioxythiophene) (PEDOT-MeOH) [46], poly(3,4-propylenedioxythiophene) (PProDOT) [85, 86], poly(3,3-diethyl-3,4-dihydro-2H-thieno-[3,4-b][1,4]diox-epine) (PProDOT-Et$_2$) [85–87], poly(2,2-dimethyl-3,4-propylenedioxythiophene) (PProDOT-Me$_2$) [85], polythiophene (PT) [33], sulfonated poly(thiophene-3-[2-(2-methoxyethoxy) ethoxy]-2,5-diyl) (s-PT) [48], polyaniline (PANI) [34], and polypyrrole (PPy) [31, 38, 39, 44, 48], and their molecular structures are shown in **Figure 6**. However, conductive polymers often showed a flat or a mesoporous structure, meaning their lacks of the directional electron transfer pathways. Because of the synthetic difficulties, very few conductive polymers can form a 0D/1D/2D structure, as listed in **Table 2**.

The hierarchical nanosphere with PPy (denoted PPy-HNS) has the hierarchical nanospherical structure with an average diameter of 100–200 nm, as shown in **Figure 7(a)** [44]. The PPy-HNS has the following photovoltaic parameters: a V_{OC} of 0.70 V, a J_{SC} of 16.49 mA cm^{-2}, a FF of 0.58, and an η of 6.71%. The nanopatterning process is one of the methods to obtain the specific structure [42]. The nanopatterned PEDOT CE shows uniform hole patterns with ~100 nm diameter (**Figure 7(b)**) and exhibits an η of 6.71%. Regardless of the nanoparticle or nanosize hole, their corresponding η values are still lower than the η of Pt CE. Therefore, there are other structures, which were synthesized to overcome the challenge.

The flexible PPy membrane is composed of nanotubes that are about 50 nm in diameter, as shown in **Figure 7(c)** [38]. The paper-like PPy membranes exhibit
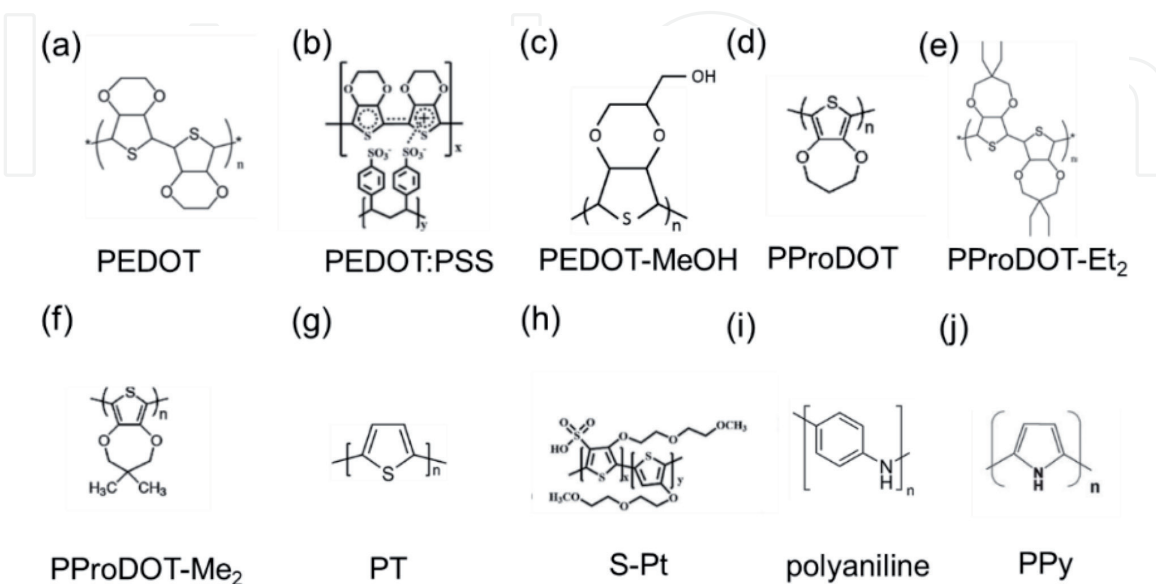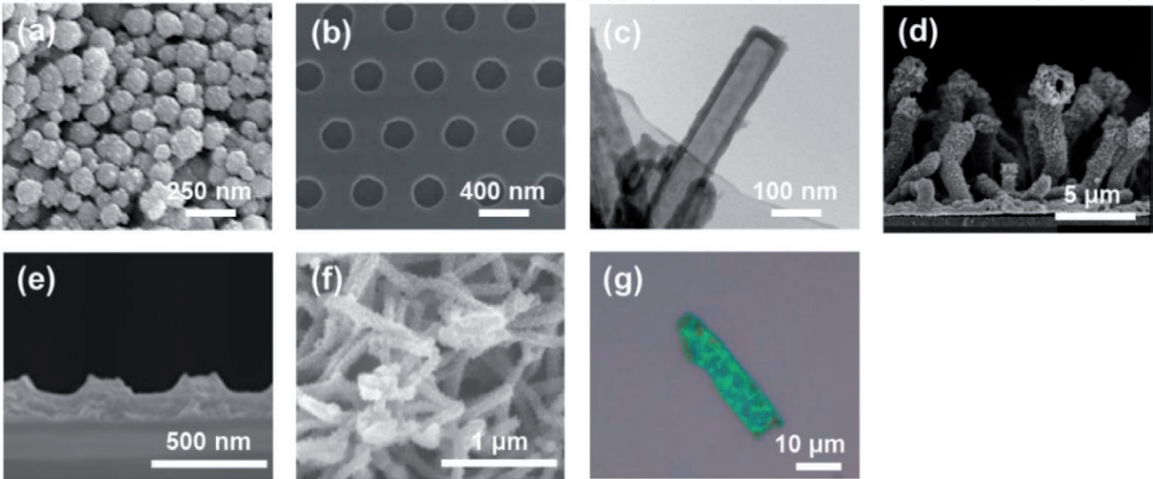

Figure 6.
The molecular structures of (a) PEDOT, (b) PEDOT:PSS [30, 43, 48], (c) PEDOT-MeOH [46], (d) PProDOT [85, 86], (e) PProDOT-Et$_2$ [85–87], (f) PProDOT-Me$_2$ [85], (g) PT [33], (h) s-PT [48], (i) PANI [34], and (j) polypyrrole (PPy) [31, 38, 39, 44, 48].

Materials	η (%)	η of Pt (%)	Structure	Ref
PPy	6.71	7.47	Hierarchical nanosphere	[44]
PEDOT	7.10	7.60	Nanosized hole	[42]
PPy	5.27	6.25	Nanotubes	[38]
PEDOT-MeOH	9.13	8.94	Tube-coral array	[46]
PEDOT	8.10	8.26	Nanorod	[35]
PANI	6.86	7.21	Nanorod	[34]
PPy	6.80	7.80	Nanosheet	[39]

Table 2.
A partial list of literature on the DSSCs with conductive polymer material-based CEs.

ηs of 5.27%, which is about 84% of the cell performance with a conventional Pt/FTO CE (6.25%). Usually, the rod structure of PEDOT is obtained by a template method. The PEDOT-MeOH tube-coral array is synthesized by a template-free and bottom-up electropolymerization technique [46]. The PEDOT-MeOH TCA shows three advantages: (1) an enhanced conjugation of the PEDOT main chain due to the electron-donating MeOH group, (2) fast one-dimensional charge transfer routes, and (3) extended electroactive sites. The PEDOT-MeOH TCA has a highly porous surface with an average length of 5 mm and an average diameter of 500 nm, as shown in **Figure 7(d)**. Besides, PEDOT-MeOH TCA has vertically grown on their FTO substrates. The PEDOT-MeOH TCA CE, the co-existence of the 1D charge transfer pathways, and large active surface area on the PEDOT-MeOH TCA give its DSSC an η of 9.13%, which is higher than the Pt CE (8.94%). This performance is rarely found in pure conductive polymer materials. The patterned PEDOT with rod is obtained by the nanopatterning procedure. It has the height of 67 nm and width of 100 nm, as shown in **Figure 7(e)** [35]. The DSSCs of patterned PEDOT exhibits an η of 8.10%, which is close to Pt CE (8.26%). The prickly polyaniline nanorods (PPNR) display a prickly nanorod structure with the diameter of ~80 nm and the length of several micrometers, as shown in **Figure 7(f)**. The PPNR CE exhibits an η of 6.86%. The ultrathin polypyrrole nanosheets (UPNSs) have a nanoscale thickness of 50 nm and sheet morphologies by using a sodium decylsulfonate template, as shown in **Figure 7(g)**. The DSSC using UPNS CE shows an η of 6.80%.
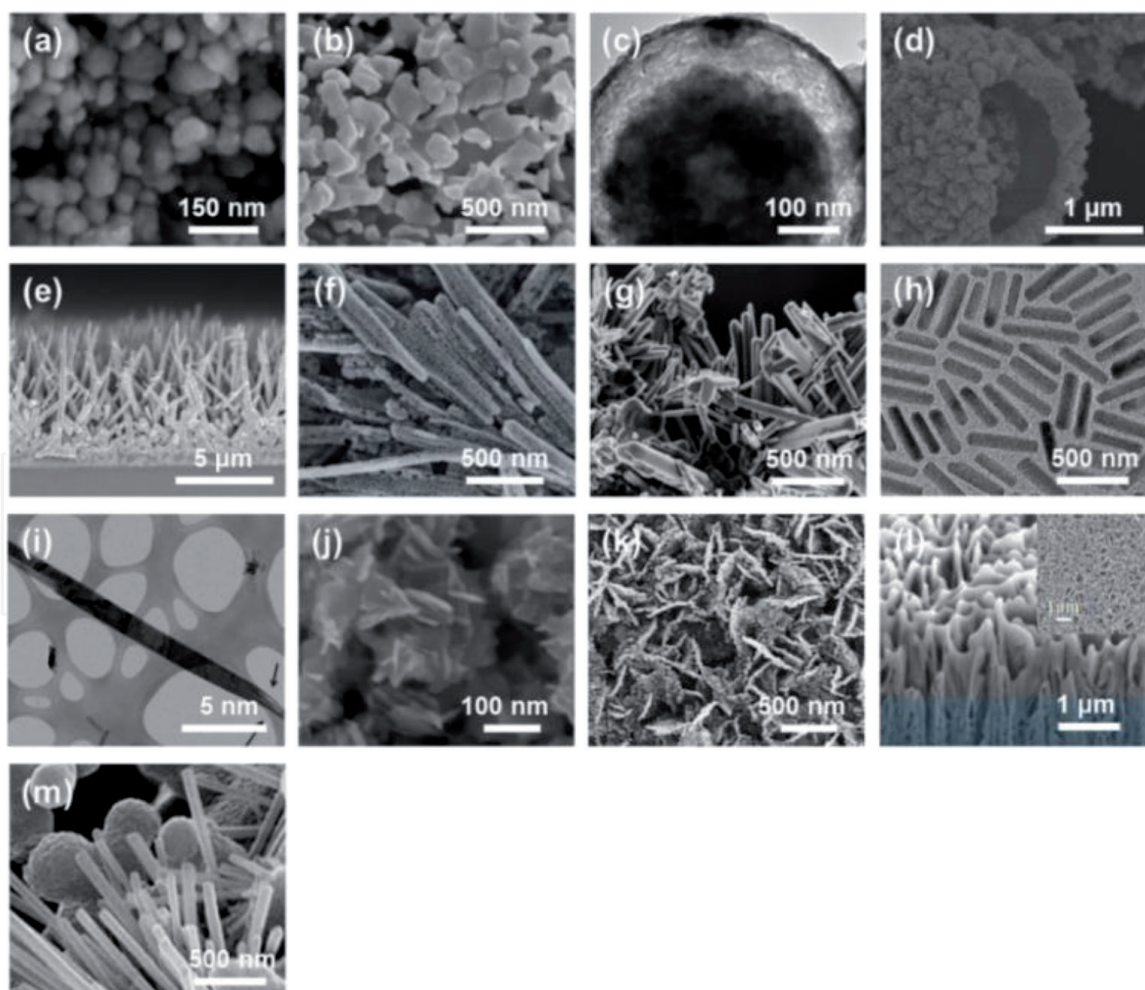

Figure 7.
The structures of conductive polymer materials include (a) hierarchical nanosphere of PPy [44], (b) nanosized hole of PEDOT [42], (c) nanotube of PPy [38], (d) hollow tubular structure of PEDOT-MeOH [46], (e) nanorod of PEDOT [35], (f) nanorod of PANI [34], and (g) nanosheet of PPy [39].

2.3 Transition metal composites

Transition metal composites (TMC) possess high potential to replace Pt CE in DSSCs because of the similar electronic structures between TMCs and Pt. Metal compounds, including carbides, nitrides, chalcogenides, oxides, phosphides, and so on, have been applied as an electrocatalyst in DSSCs to replace expensive Pt. It is still a challenge to replace Pt with TMCs due to the relatively low conductivity of TMCs. Accordingly, various TMC structures, including nanoparticle, hollow sphere, nanorod array, nanowall, hierarchical nanorod, etc., are investigated to improve the performance of TMC-based CEs, as shown in **Figure 8**. The corresponding ηs of DSSCs with various structures are listed in **Table 3**.

α-NiS has a sphere-like morphology with a diameter of 50–80 nm, as shown in **Figure 8(a)** [78]. The other NiS (β-NiS) has a nanorod 2–5 μm in length and 1000 nm in diameter. The DSSC of α-NiS CE has a better η (5.20%) than the β-NiS (η of 4.20%). The particle size of α-NiS is much smaller than nanorods of β-NiS. The smaller the size of a particle, the larger specific surface area it possesses. With the increase of specific surface area of α-NiS, the conversion efficiency reaches a higher value. The nanoparticle of $CoSe_2/CoSeO_3$ ($CoSe_2/CoSeO_3$-NP) has a diameter of 50–60 nm, as shown in **Figure 8(b)** [74]. And $CoSe_2/CoSeO_3$-NP has a larger reaction area than the nanorod and nanocube of $CoSe_2/CoSeO_3$, confirmed by the electrochemical double-layer capacitance, which is positively related to the

Figure 8.
The structures of transition metal materials including (a and b) nanoparticle [78], (c) double-shelled ball-in-ball hollow sphere [70, 74], (d) hollow spherical particle [71], (e) acicular nanorod array [49], (f–h) nanorod [53, 54, 75], (i and j) nanosheet [55, 66], (k and l) nanowall [64, 72], and (m) hierarchical nanosphere with nanorod [77].

Materials	η (%)	η of Pt (%)	Structure	Ref
NiS	5.20	6.30	Nanoparticle	[78]
$CoSe_2/CoSeO_3$	9.27	7.91	Nanoparticle	[74]
$NiCo_2S_4$	9.49	8.30	Double-shelled ball-in-ball hollow sphere	[70]
$NiCo_{0.2}@C$	9.30	8.04	Hollow spherical particle	[71]
CoS	7.67	7.70	Acicular nanorod array	[49]
MoN	7.29	7.42	Nanorod	[54]
$CoSe_2$	10.20	8.17	Nanorod	[53]
$Ni_3S_4-Pt_2Fe_1$	8.79	7.83	Nanorod	[75]
$NbSe_2$	7.73	7.01	Nanosheet	[55]
WSe_2	7.48	7.91	Nanosheet	[66]
$CoSe_2$	8.92	8.25	Nanoclimbing wall	[64]
$Cu_xZn_ySn_zS$	7.44	7.21	Nanowall	[72]
$TiO_{1.1}Se_{0.9}$	9.47	7.75	Nanosphere and nanorod	[77]

Table 3.
A partial list of literature studies on the DSSCs with conductive polymer material-based CEs. The dye of DSSCs is N719.

reaction area. The DSSC of $CoSe_2/CoSeO_3$-NP CE has an η of 9.27%, which is better than those of the nanorod and nanocube of $CoSe_2/CoSeO_3$ and is higher than that of the Pt CE (7.91%). The double-shelled hollow sphere (BHSs) structure exists in $NiCo_2S_4$ BHSs with the separation of hollow and solid parts. In **Figure 8(c)** [70], the diameter of the inner shell is 300 nm and that of the outer shell is approximately 550 nm. The thickness of the outer thin shell is 10–30 nm, which is quite less than that of the inner shell. The DSSC of $NiCo_2S_4$ BHSs CE exhibits an η of 9.49%, which is higher than that of the Pt CE (η of 8.30%). From a broken $NiCo_{0.2}@C$ micro-sphere shown in **Figure 8(d)** [71], the well-defined hollow structure with a shell thickness of around 200 nm can be observed. Meaningfully, the hollow spherical space can greatly shorten the diffusion paths within the electrode and serves as a robust reservoir for ions. The $NiCo_{0.2}@C$ exhibits an η of 9.30%, which is higher than that of the Pt CE (η of 8.04%). Most of the nanoparticles, double-shelled ball-in-ball hollow sphere, and hollow spherical particle structures have better ηs than the Pt CE.

Although TMCs present good electrocatalytic ability, the electrons may be insufficient at active sites. The rod structure is claimed to provide the specific electron transfer. It can supply sufficient electrons to keep consistent electrocatalytic reaction. From **Figure 8(e)**, it can be observed that CoS has 1D acicular nanorod arrays with the relatively rough surface of the nanorods (noted CoS ANRAs-24h) [49]. It is vertical to the FTO substrate and has a height of about 7 μm. The DSSC with CoS ANRAs-24h CE shows an η of 7.67%, which is virtually the same as the sputtered Pt-CE (η of 7.70%). The MoN nanorod (NR) on the Ti substrate has a one-dimensional structure with a diameter of 40–100 nm and a length of 0.5–2 mm, as shown in **Figure 8(f)** [54]. The electrode structure is expected to trigger positive effects on the electrochemical processes occurring in the electrode films. The MoN NR-Ti CE shows comparable performance to that using a Pt-FTO glass electrode with a V_{OC} of 0.740 V, a J_{SC} of 15.26 mA cm^{-2}, a FF of 0.65, and an η of 7.29%. The single-crystal $CoSe_2$ has nanorods 50–800 nm in length and 20–150 nm in width, as shown in **Figure 8(g)**, and possesses a lattice spacing of 3.71 ± 0.01 Å, corresponding to the

(110) planes of orthorhombic $CoSe_2$ [53]. Impressively, the single-crystal $CoSe_2$ CE produces an η of 10.20% with a V_{OC} of 0.753 V, a J_{SC} of 18.55 mA/cm^{-2}, and a FF of 0.73, which is better than the Pt CE (8.17%). The Ni_3S_4-PtFe heteronanorods are highly monodispersed with an average length of ~34.0 nm and an average diameter of 9.0 nm, as shown in **Figure 8(h)** [75]. The DSSCs using Ni_3S_4-PtFe produce an η of 8.79%, which is higher than that of the Pt CE (7.83%). The 1-D structure is obviously promoting the electrocatalytic ability of TMCs and most of the 1-D structures for TMCs exhibit a better η than Pt CE. It can be claimed that the 1-D structures of TMCs could replace the Pt CE.

The 2D structure of TMCs also has a specific electron pathway and it could be vertical to the substrate to offer sufficient electrons on active sites. Moreover, the hierarchical structure has both the advantages of a large reaction area and vertical electron pathway. For example, the direction of the fractured $NbSe_2$ sheet shows a structure with the [001] crystallographic orientation and revealed a very thick (>100 mm), disordered network arrangement of 2D sheets, as shown in **Figure 8(i)**; in comparison, the ground materials were very thin, separated nanosheets [55]. The NbSe2 sheet CE has an η of 7.73%, which reveals the potential to replace Pt CE (7.01%). The WSe_2 is composed of several interlaced nanosheets with an average thickness of approximately 15 nm and a width between 60 and 100 nm, as shown in **Figure 8(j)** [66]. The WSe_2 CE shows good electrical conductivity, subsequent energy band calculation results, and large reaction area that exhibits an η of 7.48%.

Vertically-aligned structures of electrocatalysts were reported to facilitate faster charge transport from the substrate through the electrocatalysts to the electrolyte [64, 72, 77], as shown in **Figure 9**. This structure is expected to have better electrocatalytic ability. The nanowall and the hierarchical nanorod are used with TMCs. The $CoSe_2$ nanoclimbing wall ($CoSe_2$/C-NCW) reveals arrays of vertically-aligned nanowalls with sharp edges, as shown in **Figure 8(k)** [64]. In addition, the nanowalls are covered with dot-matrix-like projections; these projections are expected to provide a large surface area to the film. On account of direct electron transfer and large surface area, the $CoSe_2$/C-NCW film, on the whole, could be a better electrocatalyst for the reduction of I_3^- to I^-, as shown in **Figure 9(a)**. The cell with $CoSe_2$/C-NCW CE reaches the highest efficiency of 8.92%, with a V_{OC} of 0.73 V, a J_{SC} of 18.03 mA cm^{-2}, and an FF of 0.67; this efficiency is even higher than that of the cell with Pt (8.25%). The CZTS nanowall electrodes (NWD) on Mo substrate show nanowalls with a width of ~500 nm, a thickness of nearly 15 nm, and a height of ~1.5 μm, which were adequately aligned in a densely packed array, which was nearly perpendicular to the surface of the Mo substrate, as shown in **Figure 8(l)** [72]. In this case, CZTS-NWD demonstrates a concept of "nano-geogrid"-reinforced CZTS nanowall electrode by synthesizing a thin layer of a porous CZTS nanostructure mimicking a geogrid on a substrate and then fabricating a CZTS nanowall on top of the nanostructure, as shown in **Figure 9(b)**. The η of the NWD device is 7.44%, which is comparable to the Pt device (7.21%). **Figure 8(m)** shows the film of
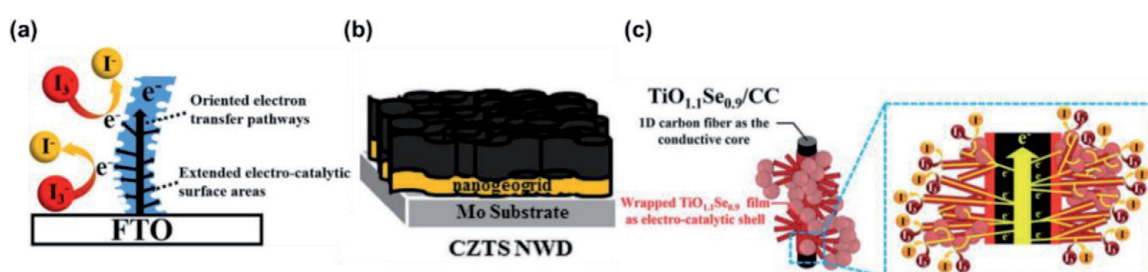
Figure 9.
The scheme of vertical aligned structures of (a and b) nanowall and (c) nanosphere with nanorod [64, 77].

$TiO_{1.1}Se_{0.9}$ wrapping around a carbon fiber, and many nanospheres and nanorods of $TiO_{1.1}Se_{0.9}$ are grown on the $TiO_{1.1}Se_{0.9}$ under-layer [77]. The $TiO_{1.1}Se_{0.9}$ nanorods are perpendicular to the surface of the carbon fiber; $TiO_{1.1}Se_{0.9}$ nanorods, therefore, are expected to facilitate a fast and 1D electron transport from the CC substrate to the interface with the electrolyte, where I_3^- reduction occurs The correctional images show the hierarchical electron transfer route electrode, where the carbon fiber in the CC serves for transporting the main stream of electrons through its 1D direction, and the deposited electrocatalysts provide secondary channels of electrons for executing the reduction of I_3^-, as shown in **Figure 9(c)**. The DSSC with the $TiO_{1.1}Se_{0.9}$–3/CC shows the best performance and gives the best η of 9.47%. Furthermore, the DSSC is used for further comparison with those cells with the Pt/CC (7.75%). In conclusion, the TMCs have good electrocatalytic ability and possess vertically aligned structures. They exhibit great ηs, which are better than that of the Pt CE.

3. Summary and future prospects

The counter electrode is a paramount part of DSSCS and has a significant influence on both the photovoltaic performance and the device cost of DSSCs. As a counter electrode, it must possess high conductivity and good catalytic activity toward electrolyte regeneration, as well as good stability. The DSSC devices employing CEs of different materials including carbon materials, conductive polymers, and transition metal composites have been summarized and discussed. One key point is that the CE performance can be optimized by combining special nanostructures into CE films to promote the industrialization of Pt-free CE catalysts. The nanostructure can briefly be classified into 0D, 1D, and 2D, which have different properties. The different materials with various nanostructures can overcome the problem of the material.

The carbon materials have numerous advantages including low cost, plasticity, simple fabrication procedures, high electrical conductivity, high thermal stability, and good corrosion resistance. The η of carbon materials has been improved by the hierarchal structures (nanotube with nanosheet and nanotube with nanoribbon) and most of the carbon materials with hierarchal structure CE have a better value of η than the traditional Pt CE. However, most of the performances of the DSSCs with carbon material CEs are still slightly lower than those DSSCs with Pt CEs. This mostly results from various resistances associated with the structurally complex carbon electrodes, such as bulk resistance through the comparatively thick carbon CE, contact resistance to the TCO substrate, the diffusion resistance in the pores of the CE, etc.

The conductive polymer materials possess outstanding electron conductivity, good adhesion, and easy fabrication. According to the literature above, it can be concluded that the 1D structure conductive polymer material-based CE can provide better η than the particles, nanosphere, and nanosheet structures. Although conductive polymer materials have larger reaction area and specific electron pathway, most of the conductive polymer material-based CEs still have a lower η than the Pt-based CEs. Only a few examples show better performance than Pt CE. It means that the conductive polymer materials need a hybrid with other electrocatalysts to obtain better electrocatalytic ability.

The TMCs exhibit great electrocatalytic ability, easy preparation, and modification. However, the poor conductivity needs to be solved in order to replace Pt CE. By synthesizing nanostructures, including nanoparticle, double-shelled ball-in-ball hollow sphere, hollow spherical particle, acicular nanorod array, nanorod, nanosheet, nanoclimbing wall, hierarchical nanorod, etc., TMCs reveal better performances than the Pt CE. It can be said that the TMCs with nanostructure successfully replace Pt CE.

Moreover, changing DSSC electrolyte toward the Cu, Co, Fe, etc. redox couples is another important research topic. Furthermore, the dim light condition application is another prospect of DSSCs. Among them, the matching material of CE is a key point to promise the η of DSSC. To get the point, it is dependent on the nanostructure and the hybrid materials, such as carbon materials with TMCs, carbon materials with conductive polymer materials, conductive polymer materials with TMCs, and TMCs with both conductive polymer materials and carbon material. Further development should focus on these main requirements: conductivity, catalytic activity, stability, efficiency, cost, and environmental friendliness. Also, the regulation mechanism for photo-induced charge carrier generation, evolution, and transportation should be of concern.

Acknowledgements

Author details

Yi-June Huang[1], Han-Ting Chen[1], Shiuan-Bai Ann[1], Chun-Ting Li[2] and Chuan-Pei Lee[3]*

1 Department of Chemical Engineering, National Taiwan University, Taiwan

2 Institute of Chemistry, Academia Sinica, Taiwan

3 Department of Applied Physics and Chemistry, University of Taipei, Taiwan

*Address all correspondence to: cplee@utaipei.edu.tw

IntechOpen

References

[1] Wu M, Ma T. Platinum-free catalysts as counter electrodes in dye-sensitized solar cells. ChemSusChem. 2012;**5**: 1343-1357. DOI: 10.1002/cssc.201100676

[2] Bella F, Gerbaldi C, Barolo C, Gratzel M. Aqueous dye-sensitized solar cells. Chemical Society Reviews. 2015;**44**:3431-3473. DOI: 10.1039/c4cs00456f

[3] Kouhnavard M, Ludin NA, Ghaffari BV, Sopian K, Ikeda S. Carbonaceous materials and their advances as a counter electrode in dye-sensitized solar cells: Challenges and prospects. ChemSusChem. 2015;**8**: 1510-1533. DOI: 10.1002/cssc.201500004

[4] Roy-Mayhew JD, Aksay IA. Graphene materials and their use in dye-sensitized solar cells. Chemical Reviews. 2014;**114**:6323-6348. DOI: 10.1021/cr400412a

[5] Lee CP, Lin CA, Wei TC, Tsai ML, Meng Y, Li CT, et al. Economical low-light photovoltaics by using the Pt-free dye-sensitized solar cell with graphene dot/PEDOT:PSS counter electrodes. Nano Energy. 2015;**18**:109-117. DOI: 10.1016/j.nanoen.2015.10.008

[6] Ganesan P, Yella A, Holcombe TW, Gao P, Rajalingam R, Al-Muhtaseb SA, et al. Unravel the impact of anchoring groups on the photovoltaic performances of diketopyrrolopyrrole sensitizers for dye-sensitized solar cells. ACS Sustainable Chemistry & Engineering. 2015;**3**:2389-2396. DOI: 10.1021/acssuschemeng.5b00332

[7] Chen CY, Jian ZH, Huang SH, Lee KM, Kao MH, Shen CH, et al. Performance characterization of dye-sensitized photovoltaics under indoor lighting. Journal of Physical Chemistry Letters. 2017;**8**:1824-1830. DOI: 10.1021/acs.jpclett.7b00515

[8] Chou HH, Liu YC, Fang G, Cao QK, Wei TC, Yeh CY. Structurally simple and easily accessible perylenes for dye-sensitized solar cells applicable to both 1 Sun and dim-light environments. ACS Applied Materials & Interfaces. 2017;**9**:37786-37796. DOI: 10.1021/acsami.7b11784

[9] Tsai MC, Wang CL, Chang CW, Hsu CW, Hsiao YH, Liu CL, et al. A large, ultra-black, efficient and cost-effective dye-sensitized solar module approaching 12% overall efficiency under 1000 lux indoor light. Journal of Materials Chemistry A. 2018;**6**: 1995-2003. DOI: 10.1039/c7ta09322e

[10] Wu M, Ma T. Recent Progress of counter electrode catalysts in dye-sensitized solar cells. The Journal of Physical Chemistry C. 2014;**118**: 16727-16742. DOI: 10.1021/jp412713h

[11] Hou Y, Wang D, Yang XH, Fang WQ, Zhang B, Wang HF, et al. Rational screening low-cost counter electrodes for dye-sensitized solar cells. Nature Communications. 2013;**4**:1583. DOI: 10.1038/ncomms2547

[12] Fan SQ, Fang B, Kim JH, Jeong B, Kim C, Yu JS, et al. Ordered multimodal porous carbon as highly efficient counter electrodes in dye-sensitized and quantum-dot solar cells. Langmuir. 2010;**26**:13644-13649. DOI: 10.1021/la1019873

[13] Xue Y, Liu J, Chen H, Wang R, Li D, Qu J, et al. Nitrogen-doped graphene foams as metal-free counter electrodes in high-performance dye-sensitized solar cells. Angewandte Chemie (International Ed. in English). 2012;**51**:12124-12127. DOI: 10.1002/anie.201207277

[14] Wang H, Sun K, Tao F, Stacchiola DJ, Hu YH. 3D honeycomb-like structured graphene and its high efficiency as a

counter-electrode catalyst for dye-sensitized solar cells. Angewandte Chemie (International Ed. in English). 2013;**52**:9210-9214. DOI: 10.1002/anie.201303497

[15] Dong P, Zhu Y, Zhang J, Hao F, Wu J, Lei S, et al. Vertically aligned carbon nanotubes/graphene hybrid electrode as a TCO- and Pt-free flexible cathode for application in solar cells. Journal of Materials Chemistry A. 2014;**2**: 20902-20907. DOI: 10.1039/c4ta05264a

[16] Ma J, Li C, Yu F, Chen J. 3 D single-walled carbon nanotube/graphene aerogels as pt-free transparent counter electrodes for high efficiency dye-sensitized solar cells. ChemSusChem. 2014;**7**:3304-3311. DOI: 10.1002/cssc.201403062

[17] Zheng X, Deng J, Wang N, Deng D, Zhang WH, Bao X, et al. Podlike N-doped carbon nanotubes encapsulating FeNi alloy nanoparticles: High-performance counter electrode materials for dye-sensitized solar cells. Angewandte Chemie (International Ed. in English). 2014;**53**:7023-7027. DOI: 10.1002/anie.201400388

[18] Wang CC, Lu SY. Carbon black-derived graphene quantum dots composited with carbon aerogel as a highly efficient and stable reduction catalyst for the iodide/tri-iodide couple. Nanoscale. 2015;**7**:1209-1215. DOI: 10.1039/c4nr06118g

[19] Yang W, Ma X, Xu X, Li Y, Raj SI, Ning G, et al. Sulfur-doped porous carbon as metal-free counter electrode for high-efficiency dye-sensitized solar cells. Journal of Power Sources. 2015;**282**:228-234. DOI: 10.1016/j.jpowsour.2015.02.060

[20] Zhang J, Yu M, Li S, Meng Y, Wu X, Liu J. Transparent conducting oxide-free nitrogen-doped graphene/reduced hydroxylated carbon nanotube composite paper as flexible counter electrodes for dye-sensitized solar cells. Journal of Power Sources. 2016;**334**:44-51. DOI: 10.1016/j.jpowsour.2016.10.012

[21] Memon AA, Arbab AA, Sahito IA, Sun KC, Mengal N, Jeong SH. Synthesis of highly photo-catalytic and electro-catalytic active textile structured carbon electrode and its application in DSSCs. Solar Energy. 2017;**150**:521-531. DOI: 10.1016/j.solener.2017.04.052

[22] Tseng CA, Lee CP, Huang YJ, Pang HW, Ho KC, Chen YT. One-step synthesis of graphene hollow nanoballs with various nitrogen-doped states for electrocatalysis in dye-sensitized solar cells. Materials Today Energy. 2018;**8**: 15-21. DOI: 10.1016/j.mtener.2018.02.006

[23] Lee CP, Lai KY, Lin CA, Li CT, Ho KC, Wu CI, et al. A paper-based electrode using a graphene dot/PEDOT:PSS composite for flexible solar cells. Nano Energy. 2017;**36**:260-267. DOI: 10.1016/j.nanoen.2017.04.044

[24] Li CT, Lee CT, Li SR, Lee CP, Chiu IT, Vittal R, et al. Composite films of carbon black nanoparticles and sulfonated-polythiophene as flexible counter electrodes for dye-sensitized solar cells. Journal of Power Sources. 2016;**302**:155-163. DOI: 10.1016/j.jpowsour.2015.10.028

[25] Li YY, Li CT, Yeh MH, Huang KC, Chen PW, Vittal R, et al. Graphite with different structures as catalysts for counter electrodes in dye-sensitized solar cells. Electrochimica Acta. 2015;**179**:211-219. DOI: 10.1016/j.electacta.2015.06.007

[26] Chen PY, Li CT, Lee CP, Vittal R, Ho KC. PEDOT-decorated nitrogen-doped graphene as the transparent composite film for the counter electrode of a dye-sensitized solar cell. Nano Energy. 2015;**12**:374-385. DOI: 10.1016/j.nanoen.2015.01.010

[27] Yeh MH, Lin LY, Sun CL, Leu YA, Tsai JT, Yeh CY, et al. Multiwalled

carbon nanotube@reduced graphene oxide nanoribbon as the counter electrode for dye-sensitized solar cells. The Journal of Physical Chemistry C. 2014;**118**:16626-16634. DOI: 10.1021/jp412542d

[28] Lin CA, Lee CP, Ho ST, Wei TC, Chi YW, Huang KP, et al. Nitrogen-doped Graphene/platinum counter electrodes for dye-sensitized solar cells. ACS Photonics. 2014;**1**:1264-1269. DOI: 10.1021/ph500219r

[29] Groenendaal_et_al-2000-Advanced_Materials.pdf. DOI: 10.1002/(SICI)1521-4095(200004)12:73.3.CO;2-3

[30] Xia J, Masaki N, Jiang K, Yanagida S. The influence of doping ions on poly(3,4-ethylenedioxythiophene) as a counter electrode of a dye-sensitized solar cell. Journal of Materials Chemistry. 2007;**17**:2845. DOI: 10.1039/b703062b

[31] Xia J, Chen L, Yanagida S. Application of polypyrrole as a counter electrode for a dye-sensitized solar cell. Journal of Materials Chemistry. 2011;**21**:4644. DOI: 10.1039/c0jm04116e

[32] Zhang R, Li Z, Xu J, Xia J. Synthesis and application of poly(bis-3,4-ethylenedioxythiophene methine)s as novel counter electrodes in dye-sensitized solar cells. Solar Energy. 2018;**173**:1189-1196. DOI: 10.1016/j.solener.2018.08.063

[33] Wu J, Lan Z, Lin J, Huang M, Huang Y, Fan L, et al. Counter electrodes in dye-sensitized solar cells. Chemical Society Reviews. 2017;**46**:5975-6023. DOI: 10.1039/c6cs00752j

[34] Wang G, Yan C, Zhang W. Prickly polyaniline nano/microstructures as the efficient counter electrode materials for dye-sensitized solar cells. Journal of Nanoparticle Research. 2017;**19**:395. DOI: 10.1007/s11051-017-4087-0

[35] Park C, Na J, Kim E. Cross stacking of nanopatterned PEDOT films for use as soft electrodes. ACS Applied Materials & Interfaces. 2017;**9**:28802-28809. DOI: 10.1021/acsami.7b07799

[36] Li H, Xiao Y, Han G, Hou W. Honeycomb-like poly(3,4-ethylenedioxythiophene) as an effective and transparent counter electrode in bifacial dye-sensitized solar cells. Journal of Power Sources. 2017;**342**:709-716. DOI: 10.1016/j.jpowsour.2017.01.007

[37] Yun S, Hagfeldt A, Ma T. Pt-free counter electrode for dye-sensitized solar cells with high efficiency. Advanced Materials. 2014;**26**:6210-6237. DOI: 10.1002/adma.201402056

[38] Peng T, Sun W, Huang C, Yu W, Sebo B, Dai Z, et al. Self-assembled free-standing polypyrrole nanotube membrane as an efficient FTO- and Pt-free counter electrode for dye-sensitized solar cells. ACS Applied Materials & Interfaces. 2014;**6**:14-17. DOI: 10.1021/am404265q

[39] Hwang DK, Song D, Jeon SS, Han TH, Kang YS, Im SS. Ultrathin polypyrrole nanosheets doped with HCl as counter electrodes in dye-sensitized solar cells. Journal of Materials Chemistry A. 2014;**2**:859-865. DOI: 10.1039/c3ta13367b

[40] Carli S, Casarin L, Bergamini G, Caramori S, Bignozzi CA. Conductive PEDOT covalently bound to transparent FTO electrodes. The Journal of Physical Chemistry C. 2014;**118**:16782-16790. DOI: 10.1021/jp412758g

[41] Kwon J, Park NG, Lee JY, Ko MJ, Park JH. Highly efficient monolithic dye-sensitized solar cells. ACS Applied Materials & Interfaces. 2013;**5**:2070-2074. DOI: 10.1021/am302974z

[42] Kwon J, Ganapathy V, Kim YH, Song KD, Park HG, Jun Y, et al.

Nanopatterned conductive polymer films as a Pt, TCO-free counter electrode for low-cost dye-sensitized solar cells. Nanoscale. 2013;**5**:7838-7843. DOI: 10.1039/c3nr01294h

[43] Zhang TL, Chen HY, Su CY, Kuang DB. A novel TCO- and Pt-free counter electrode for high efficiency dye-sensitized solar cells. Journal of Materials Chemistry A. 2013;**1**: 1724-1730. DOI: 10.1039/c2ta00974a

[44] Chang LY, Li CT, Li YY, Lee CP, Yeh MH, Ho KC, et al. Morphological influence of polypyrrole nanoparticles on the performance of dye–sensitized solar cells. Electrochimica Acta. 2015;**155**:263-271. DOI: 10.1016/j.electacta.2014.12.127

[45] Li CT, Chang HY, Li YY, Huang YJ, Tsai YL, Vittal R, et al. Electrocatalytic zinc composites as the efficient counter electrodes of dye-sensitized solar cells: Study on the electrochemical performances and density functional theory calculations. ACS Applied Materials & Interfaces. 2015;**7**:28254-28263. DOI: 10.1021/acsami.5b07724

[46] Lin YF, Li CT, Ho KC. A template-free synthesis of the hierarchical hydroxymethyl PEDOT tube-coral array and its application in dye-sensitized solar cells. Journal of Materials Chemistry A. 2016;**4**:384-394. DOI: 10.1039/c5ta06376k

[47] Tsai CH, Huang WC, Hsu YC, Shih CJ, Teng IJ, Yu YH. Poly (o-methoxyaniline) doped with an organic acid as cost-efficient counter electrodes for dye-sensitized solar cells. Electrochimica Acta. 2016;**213**:791-801. DOI: 10.1016/j.electacta.2016.08.012

[48] Li CT, Lin YF, Chiu IT, Ho KC. TCO-free conducting polymers/carbon cloths as the flexible electro-catalytic counter electrodes for dye-sensitized solar cells. Journal of Materials Chemistry

A. 2015;**3**:24479-24486. DOI: 10.1039/c5ta06382e

[49] 2012 CoS Acicular Nanorod Arrays for the.pdf

[50] Wu M, Lin X, Wang Y, Wang L, Guo W, Qi D, et al. Economical Pt-free catalysts for counter electrodes of dye-sensitized solar cells. Journal of the American Chemical Society. 2012;**134**:3419-3428. DOI: 10.1021/ja209657v

[51] Zhou H, Shi Y, Dong Q, Wang L, Zhang H, Ma T. High electrocatalytic activity of W18O49 nanowires for cobalt complex and ferrocenium redox mediators. RSC Advances. 2014;**4**:42190-42196. DOI: 10.1039/c4ra07906j

[52] Yang X, Zhou L, Feng A, Tang H, Zhang H, Ding Z, et al. Synthesis of nickel sulfides of different phases for counter electrodes in dye-sensitized solar cells by a solvothermal method with different solvents. Journal of Materials Research. 2014;**29**:935-941. DOI: 10.1557/jmr.2014.74

[53] Sun H, Zhang L, Wang Z-S. Single-crystal CoSe$_2$ nanorods as an efficient electrocatalyst for dye-sensitized solar cells. Journal of Materials Chemistry A. 2014;**2**:16023-16029. DOI: 10.1039/c4ta02238f

[54] Song J, Li GR, Xi K, Lei B, Gao XP, Kumar RV. Enhancement of diffusion kinetics in porous MoN nanorods-based counter electrode in a dye-sensitized solar cell. Journal of Materials Chemistry A. 2014;**2**:10041. DOI: 10.1039/c4ta01342e

[55] Ibrahem MA, Huang W-C, Lan T-W, Boopathi KM, Hsiao Y-C, Chen C-H, et al. Controlled mechanical cleavage of bulk niobium diselenide to nanoscaled sheet, rod, and particle structures for Pt-free dye-sensitized solar cells. Journal of Materials Chemistry A. 2014;**2**:11382-11390. DOI: 10.1039/c4ta01881h

[56] Hsu SH, Li CT, Chien HT, Salunkhe RR, Suzuki N, Yamauchi Y, et al. Platinum-free counter electrode comprised of metal-organic-framework (MOF)-derived cobalt sulfide nanoparticles for efficient dye-sensitized solar cells (DSSCs). Scientific Reports. 2014;**4**:6983. DOI: 10.1038/srep06983

[57] Zhou L, Zhuang Z, Zhao H, Lin M, Zhao D, Mai L. Intricate hollow structures: Controlled synthesis and applications in energy storage and conversion. Advanced Materials. 2017;**29**(20):1602914. DOI: 10.1002/adma.201602914

[58] Singh E, Kim KS, Yeom GY, Nalwa HS. Two-dimensional transition metal dichalcogenide-based counter electrodes for dye-sensitized solar cells. RSC Advances. 2017;**7**:28234-28290. DOI: 10.1039/c7ra03599c

[59] Dong F, Guo Y, Xu P, Yin X, Li Y, He M. Hydrothermal growth of MoS_2/Co_3S_4 composites as efficient Pt-free counter electrodes for dye-sensitized solar cells. Science China Materials. 2017;**60**:295-303. DOI: 10.1007/s40843-017-9009-8

[60] Chen TY, Huang YJ, Li CT, Kung CW, Vittal R, Ho KC. Metal-organic framework/sulfonated polythiophene on carbon cloth as a flexible counter electrode for dye-sensitized solar cells. Nano Energy. 2017;**32**:19-27. DOI: 10.1016/j.nanoen.2016.12.019

[61] Infant RS, Xu X, Yang W, Yang F, Hou L, Li Y. Highly active and reflective MoS_2 counter electrode for enhancement of photovoltaic efficiency of dye sensitized solar cells. Electrochimica Acta. 2016;**212**:614-620. DOI: 10.1016/j.electacta.2016.07.059

[62] Li CT, Tsai YL, Ho KC. Earth abundant silicon composites as the electrocatalytic counter electrodes for dye-sensitized solar cells. ACS Applied Materials & Interfaces. 2016;**8**:7037-7046. DOI: 10.1021/acsami.5b12423

[63] Fan MS, Lee CP, Li CT, Huang YJ, Vittal R, Ho KC. Nitrogen-doped graphene/molybdenum disulfide composite as the electrocatalytic film for dye-sensitized solar cells. Electrochimica Acta. 2016;**211**:164-172. DOI: 10.1016/j.electacta.2016.06.047

[64] Chiu IT, Li CT, Lee CP, Chen PY, Tseng YH, Vittal R, et al. Nanoclimbing-wall-like $CoSe_2$/carbon composite film for the counter electrode of a highly efficient dye-sensitized solar cell: A study on the morphology control. Nano Energy. 2016;**22**:594-606. DOI: 10.1016/j.nanoen.2016.02.060

[65] Antonelou A, Syrrokostas G, Sygellou L, Leftheriotis G, Dracopoulos V, Yannopoulos SN. Facile, substrate-scale growth of mono- and few-layer homogeneous MoS_2 films on Mo foils with enhanced catalytic activity as counter electrodes in DSSCs. Nanotechnology. 2016;**27**:045404. DOI: 10.1088/0957-4484/27/4/045404

[66] Guo J, Liang S, Shi Y, Hao C, Wang X, Ma T. Transition metal selenides as efficient counter-electrode materials for dye-sensitized solar cells. Physical Chemistry Chemical Physics. 2015;**17**:28985-28992. DOI: 10.1039/c5cp04862a

[67] <2018 The Dye-Sensitized Solar Cells Based on the Interconnected Ternary Cobalt Diindium Sulfide Nanosheet Array Counter Electrode.pdf>

[68] Su L, Xiao Y, Han G, Lin J-Y. One-step hydrothermal synthesis of feather duster-like $NiS@MoS_2$ with hierarchical array structure for the Pt-free dye-sensitized solar cell. Journal of Nanoparticle Research. 2018;**20**:115. DOI: 10.1007/s11051-018-4223-5

[69] Prasad S, Durai G, Devaraj D, AlSalhi MS, Theerthagiri J, Arunachalam P, et al.

3D nanorhombus nickel nitride as stable and cost-effective counter electrodes for dye-sensitized solar cells and supercapacitor applications. RSC Advances. 2018;**8**:8828-8835. DOI: 10.1039/c8ra00347e

[70] Jiang Y, Qian X, Zhu C, Liu H, Hou L. Nickel cobalt sulfide double-shelled hollow nanospheres as superior bifunctional electrocatalysts for photovoltaics and alkaline hydrogen evolution. ACS Applied Materials & Interfaces. 2018;**10**:9379-9389. DOI: 10.1021/acsami.7b18439

[71] Jiang X, Li H, Li S, Huang S, Zhu C, Hou L. Metal-organic framework-derived Ni–Co alloy@carbon microspheres as high-performance counter electrode catalysts for dye-sensitized solar cells. Chemical Engineering Journal. 2018;**334**:419-431. DOI: 10.1016/j.cej.2017.10.043

[72] Chiu JM, Chen EM, Lee CP, Shown I, Tunuguntla V, Chou JS, et al. Geogrid-inspired nanostructure to reinforce a CuxZnySnzS nanowall electrode for high-stability electrochemical energy conversion devices. Advanced Materials. 2017;**7**:1602210. DOI: 10.1002/aenm.201602210

[73] Jian SL, Huang YJ, Yeh MH, Ho KC. A zeolitic imidazolate framework-derived ZnSe/N-doped carbon cube hybrid electrocatalyst as the counter electrode for dye-sensitized solar cells. Journal of Materials Chemistry A. 2018;**6**:5107-5118. DOI: 10.1039/c8ta00968f

[74] Huang YJ, Lee CP, Pang HW, Li CT, Fan MS, Vittal R, et al. Microemulsion-controlled synthesis of $CoSe_2/CoSeO_3$ composite crystals for electrocatalysis in dye-sensitized solar cells. Materials Today Energy. 2017;**6**:189-197. DOI: 10.1016/j.mtener.2017.10.004

[75] Huang S, Ma D, Hu Z, He Q, Zai J, Chen D, et al. Synergistically enhanced electrochemical performance of Ni3S4-PtX (X = Fe, Ni) heteronanorods as heterogeneous catalysts in dye-sensitized solar cells. ACS Applied Materials & Interfaces. 2017;**9**:27607-27617. DOI: 10.1021/acsami.7b05418

[76] Huang YJ, Fan MS, Li CT, Lee CP, Chen TY, Vittal R, et al. $MoSe_2$ nanosheet/poly(3,4-ethylenedioxythiophene): Poly(styrenesulfonate) composite film as a Pt-free counter electrode for dye-sensitized solar cells. Electrochimica Acta. 2016;**211**:794-803. DOI: 10.1016/j.electacta.2016.06.086

[77] Li CT, Lee CP, Chiu IT, Vittal R, Huang YJ, Chen TY, et al. Hierarchical TiO1.1Se0.9-wrapped carbon cloth as the TCO-free and Pt-free counter electrode for iodide-based and cobalt-based dye-sensitized solar cells. Journal of Materials Chemistry A. 2017;**5**:14079-14091. DOI: 10.1039/c7ta02474f

[78] Chuang HM, Li CT, Yeh MH, Lee CP, Vittal R, Ho KC. A coral-like film of Ni@NiS with core–shell particles for the counter electrode of an efficient dye-sensitized solar cell. Journal of Materials Chemistry A. 2014;**2**:5816-5824. DOI: 10.1039/c4ta00011k

[79] Lee CT, Peng JD, Li CT, Tsai YL, Vittal R, Ho KC. Ni_3Se_4 hollow architectures as catalytic materials for the counter electrodes of dye-sensitized solar cells. Nano Energy. 2014;**10**:201-211. DOI: 10.1016/j.nanoen.2014.09.017

[80] Shiraz HG, Astaraie FR. Carbonaceous materials as substitutes for conventional dye-sensitized solar cell counter electrodes. Journal of Materials Chemistry A. 2015;**3**:20849-20862. DOI: 10.1039/c5ta02840j

[81] Batmunkh M, Biggs MJ, Shapter JG. Carbon nanotubes for dye-sensitized solar cells. Small. 2015;**11**:2963-2989. DOI: 10.1002/smll.201403155

[82] Bi H, Cui H, Lin T, Huang F. Graphene wrapped copper–nickel nanospheres on highly conductive graphene film for use as counter electrodes of dye-sensitized solar cells. Carbon. 2015;**91**:153-160. DOI: 10.1016/j.carbon.2015.04.051

[83] Xu Y, Fleischer AS, Feng G. Reinforcement and shape stabilization of phase-change material via graphene oxide aerogel. Carbon. 2017;**114**:334-346. DOI: 10.1016/j.carbon.2016.11.069

[84] Zhang X, Sui Z, Xu B, Yue S, Luo Y, Zhan W, et al. Mechanically strong and highly conductive graphene aerogel and its use as electrodes for electrochemical power sources. Journal of Materials Chemistry. 2011;**21**:6494. DOI: 10.1039/c1jm10239g

[85] Ahmad S, Bessho T, Kessler F, Baranoff E, Frey J, Yi C, et al. A new generation of platinum and iodine free efficient dye-sensitized solar cells. Physical Chemistry Chemical Physics. 2012;**14**:10631-10639. DOI: 10.1039/c2cp41611e

[86] Lee KM, Chen PE, Hsu CU, Huang JS, Ho WS, Chen HH, et al. A high-performance counter electrode based on poly(3,4-alkylenedioxythiophene) for dye-sensitized solar cells. Journal of Power Sources. 2009;**188**:313-318. DOI: 10.1016/j.jpowsour.2008.11.075

[87] Yeh MH, Lee CP, Lin LY, Nien PC, Chen PY, Vittal R, et al. A composite poly(3,3-diethyl-3,4-dihydro-2H-thieno-[3,4-b][1,4]-dioxepine) and Pt film as a counter electrode catalyst in dye-sensitized solar cells. Electrochimica Acta. 2011;**56**:6157-6164. DOI: 10.1016/j.electacta.2011.04.028